BRAIN
A JOURNAL OF NEUROLOGY

Biallelic *MADD* variants cause a phenotypic spectrum ranging from developmental delay to a multisystem disorder

Pauline E. Schneeberger,[1] Fanny Kortüm,[1] Georg Christoph Korenke,[2] Malik Alawi,[3] René Santer,[4] Mathias Woidy,[4] Daniela Buhas,[5,6] Stephanie Fox,[5,6] Jane Juusola,[7] Majid Alfadhel,[8,9,10] Bryn D. Webb,[11,12,13] Emanuele G. Coci,[14,15] Rami Abou Jamra,[16] Manuela Siekmeyer,[17] Saskia Biskup,[18] Corina Heller,[18] Esther M. Maier,[19] Poupak Javaher-Haghighi,[20] Maria F. Bedeschi,[21] Paola F. Ajmone,[22] Maria Iascone,[23] Hilde Peeters,[24] Katleen Ballon,[25] Jaak Jaeken,[26] Aroa Rodríguez Alonso,[27] María Palomares-Bralo,[28] Fernando Santos-Simarro,[28] Marije E.C. Meuwissen,[29] Diane Beysen,[30] R. Frank Kooy,[31] Henry Houlden,[32] David Murphy,[32] Mohammad Doosti,[33] Ehsan G. Karimiani,[33,34] Majid Mojarrad,[35,36,37] Reza Maroofian,[32] Lenka Noskova,[38] Stanislav Kmoch,[38] Tomas Honzik,[39] Heidi Cope,[40] Amarilis Sanchez-Valle,[41] Undiagnosed Diseases Network,[#] Bruce D. Gelb,[11,12,13] Ingo Kurth,[42,43] Maja Hempel[1,*] and Kerstin Kutsche[1,*]

*These authors contributed equally to this work.

#Appendix 1.

In pleiotropic diseases, multiple organ systems are affected causing a variety of clinical manifestations. Here, we report a pleiotropic disorder with a unique constellation of neurological, endocrine, exocrine, and haematological findings that is caused by biallelic *MADD* variants. MADD, the mitogen-activated protein kinase (MAPK) activating death domain protein, regulates various cellular functions, such as vesicle trafficking, activity of the Rab3 and Rab27 small GTPases, tumour necrosis factor-α (TNF-α)-induced signalling and prevention of cell death. Through national collaboration and GeneMatcher, we collected 23 patients with 21 different pathogenic *MADD* variants identified by next-generation sequencing. We clinically evaluated the series of patients and categorized the phenotypes in two groups. Group 1 consists of 14 patients with severe developmental delay, endo- and exocrine dysfunction, impairment of the sensory and autonomic nervous system, and haematological anomalies. The clinical course during the first years of life can be potentially fatal. The nine patients in Group 2 have a predominant neurological phenotype comprising mild-to-severe developmental delay, hypotonia, speech impairment, and seizures. Analysis of mRNA revealed multiple aberrant *MADD* transcripts in two patient-derived fibroblast cell lines. Relative quantification of MADD mRNA and protein in fibroblasts of five affected individuals showed a drastic reduction or loss of MADD. We conducted functional tests to determine the impact of the variants on different pathways. Treatment of patient-derived fibroblasts with TNF-α resulted in reduced phosphorylation of the extracellular signal-regulated kinases 1 and 2, enhanced activation of the pro-apoptotic enzymes caspase-3 and -7 and increased apoptosis compared to control cells. We analysed internalization of epidermal growth factor in patient cells and identified a defect in endocytosis of epidermal growth factor. We conclude that MADD deficiency underlies multiple cellular defects that can be attributed to alterations of TNF-α-dependent signalling pathways and defects in vesicular trafficking. Our data highlight the multi-faceted role of MADD as a signalling molecule in different organs and reveal its physiological role in regulating the function of the sensory and autonomic nervous system and endo- and exocrine glands.

1 Institute of Human Genetics, University Medical Center Hamburg-Eppendorf, Hamburg, Germany
2 Klinik für Neuropädiatrie und angeborene Stoffwechselerkrankungen, Klinikum Oldenburg, Oldenburg, Germany
3 Bioinformatics Core Unit, University Medical Center Hamburg-Eppendorf, Hamburg, Germany
4 Department of Pediatrics, University Medical Center Hamburg-Eppendorf, Hamburg, Germany
5 Division of Medical Genetics, Department of Specialized Medicine, McGill University Health Centre, Montreal, Canada
6 Human Genetics Department, McGill University, Montreal, Canada
7 GeneDx, Gaithersburg, USA
8 Division of Genetics, Department of Pediatrics, King Abdullah specialized Children's Hospital, King Abdulaziz Medical City, Ministry of National Guard-Health Affairs (MNGHA), Riyadh, Saudi Arabia
9 Medical Genomics Research Department, King Abdullah International Medical Research Center (KAIMRC), Ministry of National Guard-Health Affairs (MNGHA), Riyadh, Saudi Arabia
10 King Saud Bin Abdulaziz University for Health Sciences, Ministry of National Guard-Health Affairs (MNGHA), Riyadh, Saudi Arabia
11 Department of Genetics and Genomic Sciences, Icahn School of Medicine at Mount Sinai, New York, USA
12 Department of Pediatrics, Icahn School of Medicine at Mount Sinai, New York, USA
13 Mindich Child Health and Development Institute, Icahn School of Medicine at Mount Sinai, New York, USA
14 Department for Neuropediatrics, University Children's Hospital, Ruhr University Bochum, Bochum, Germany
15 Department of Pediatrics, Prignitz Hospital, Brandenburg Medical School, Germany
16 Institute of Human Genetics, University Medical Center Leipzig, Leipzig, Germany
17 Universitätsklinikum Leipzig - AöR, University of Leipzig, Hospital for Children and Adolescents, Leipzig, Germany
18 CeGaT GmbH and Praxis für Humangenetik Tübingen, Tübingen, Germany
19 Dr. von Hauner Children's Hospital, University of Munich, Munich, Germany
20 Medicover Humangenetik Hannover, Hanover, Germany
21 Medical Genetic Unit, Fondazione IRCCS Ca' Granda Ospedale Maggiore Policlinico, Milan, Italy
22 Child and Adolescent Neuropsychiatric Unit, Fondazione IRCCS Cà Granda Ospedale Maggiore Policlinico, Milan, Italy
23 Laboratorio di Genetica Medica, ASST Papa Giovanni XXIII, Bergamo, Italy
24 Center for Human Genetics, KU Leuven, Leuven, Belgium
25 Centre for Developmental Disabilities, Department of Development and Regeneration, KU Leuven, Leuven, Belgium
26 Center for Metabolic Diseases, KU Leuven, Leuven, Belgium
27 Unidad de Patología Compleja, Servicio de Pediatría, Hospital Universitario La Paz, Madrid, Spain
28 Instituto de Genética Médica y Molecular (INGEMM), Hospital Universitario La Paz, IdiPAZ, CIBERER, ISCIII, Madrid, Spain
29 Center of Medical Genetics, University Hospital Antwerp, Antwerp, Belgium
30 Department of Pediatric Neurology, University Hospital Antwerp, Antwerp, Belgium
31 Department of Medical Genetics, University of Antwerp, Antwerp, Belgium
32 Department of Neuromuscular Diseases, UCL Queen Square Institute of Neurology and The National Hospital for Neurology and Neurosurgery, London, UK
33 Next Generation Genetic Polyclinic, Mashhad, Iran
34 Genetics Research Centre, Molecular and Clinical Sciences Institute, St. George's, University, London, UK
35 Department of Medical Genetics, Faculty of Medicine, Mashhad University of Medical Sciences, Mashhad, Iran
36 Medical Genetics Research Center, Mashhad University of Medical Sciences, Mashhad, Iran
37 Genetic Center of Khorasan Razavi, Mashhad, Iran
38 Research Unit for Rare Diseases, Department of Pediatrics and Adolescent Medicine, First Faculty of Medicine, Charles University, Prague, Czech Republic
39 Department of Pediatrics and Adolescent Medicine, First Faculty of Medicine, Charles University and General University Hospital, Prague, Czech Republic
40 Division of Medical Genetics, Department of Pediatrics, Duke University Medical Center, Durham, North Carolina, USA
41 Division of Genetics and Metabolism, College of Medicine, University of South Florida, Tampa, Florida, USA
42 Institute of Human Genetics, Medical Faculty, RWTH Aachen University, Aachen, Germany
43 Institute of Human Genetics, Jena University Hospital, Jena, Germany

Correspondence to: Kerstin Kutsche, PhD
Institute of Human Genetics
University Medical Center Hamburg-Eppendorf
Martinistraße 52
20246 Hamburg
Germany
E-mail: kkutsche@uke.de

Introduction

MADD encoding the MAPK-activating protein containing a death domain (or MAP kinase activating death domain) belongs to the DENN (differentially expressed normal versus neoplastic) domain protein families in humans, which are regulators of Rab family members of small GTPases. The tripartite DENN domain consists of a central DENN module flanked by upstream and downstream modules (uDENN and dDENN). In the C-terminal region, MADD has a serine-rich domain and a death domain (Marat *et al.*, 2011). Originally, MADD (alternative name RAB3 GEP) was identified as a guanine nucleotide exchange factor (GEF) for Rab3 that mediates the exchange of GDP for GTP and thereby activates Rab3 (Wada *et al.*, 1997). Rab3 is present on synaptic vesicles and important for Ca^{2+}-dependent exocytosis of neurotransmitter release (Geppert *et al.*, 1994). MADD upregulates a post-docking step of synaptic exocytosis (Yamaguchi *et al.*, 2002) and, by binding to the kinesins KIF1Bβ and KIF1A, MADD mediates motor-dependent transport of GTP-Rab3-positive vesicles to the presynaptic nerve terminals (Niwa *et al.*, 2008). Collectively, the data demonstrate that MADD can act both as a Rab3 GEF and Rab3 effector and plays a role in formation and trafficking of synaptic vesicles. Besides MADD's function in neurotransmission, the DENN and death domain of MADD interact with the type 1 tumour necrosis factor receptor (TNFR1) (Schievella *et al.*, 1997; Coppola *et al.*, 2002), thereby stimulating TNFR1-dependent activation of the MAP kinases ERK and JNK and/or the transcription factor NF-κB (Schievella *et al.*, 1997; Murakami-Mori *et al.*, 1999; Al-Zoubi *et al.*, 2001; Kurada *et al.*, 2009). Under stress conditions that are mediated by tumour necrosis factor-α (TNF-α), MADD has been proposed to exchange binding partners by switching from binding to Rab proteins to TNFR1 (Miyoshi and Takai, 2004).

The *MADD* pre-mRNA undergoes extensive splicing leading to expression of at least seven different isoforms (Supplementary Fig. 1) (Al-Zoubi *et al.*, 2001; Efimova *et al.*, 2004). IG20, MADD/DENN (IG20-SV1), IG20-SV2, and DENN-SV (IG20-SV3) are ubiquitously expressed in human tissues, while expression of IG20-SV4 and KIAA0358 is restricted to certain neuronal tissues, such as cerebral cortex and hippocampus (Al-Zoubi *et al.*, 2001; Efimova *et al.*, 2004; Li *et al.*, 2008). The different MADD isoforms have differential roles in cell survival. For example, IG20 and IG20-SV4 have pro-apoptotic effects, while MADD/DENN, DENN-SV and KIAA0358 isoforms protect against apoptosis upon TNF-α treatment (Al-Zoubi *et al.*, 2001; Li *et al.*, 2008; Kurada *et al.*, 2009). MADD was found to be overexpressed in cancer cells and tissues and contributes to cancer cell survival by protecting cells from spontaneous, TNF-α- and TRAIL- (TNF-α-related apoptosis-inducing ligand) induced apoptosis (Chow and Lee, 1996; Lim *et al.*, 2004; Mulherkar *et al.*, 2006, 2007; Kurada *et al.*, 2009).

In this study, based on an initial discovery from whole-exome sequencing (WES) in two siblings with a multisystem disorder, we subsequently assembled a set of 23 individuals carrying homozygous or compound heterozygous variants in *MADD*. We delineated the variable phenotypes and describe a clinical spectrum ranging from mild developmental delay to a severe pleiotropic disorder with the distinguishing hallmarks of severe developmental delay, sensory and autonomic dysfunction, exocrine and endocrine insufficiency, and haematological anomalies. Early death occurred in seven patients. We characterized the underlying biochemical consequences of MADD deficiency in patient-derived fibroblasts, demonstrating multiple cellular defects that can be attributed to alterations of TNF-α-dependent signalling pathways and defects in vesicular trafficking.

Materials and methods

Patients

Informed consent for genetic analyses was obtained for all patients, and genetic studies were performed clinically or as approved by the Institutional Review Boards of the relevant institutions. The patients' parents provided written informed consent for the participation in the study, clinical data and specimen collection, genetic analysis and publication of relevant findings. Permission to publish photographs was provided for patients shown in Fig. 4.

Next-generation sequencing

Quad whole-genome sequencing (WGS) was performed in Family 11 (Patients 13, 14 and parents). Quad WES was carried out in Family 13 (Patients 16, 17 and parents), trio WES (patient and parents) in Families 2 (Patient 4), 3, 6, 7, 8, 10, 12 and 17, duo WES in Families 1 (Patients 1 and 2) and 5 (Patient 7 and mother), and single WES in Patients 11 (Family 9), 20 (Family 15), and 21 (Family 16). Exome sequencing in Family 4 (Patient 6) has been previously reported (Anazi *et al.*, 2017). Mendeliome gene panel (6178 genes) was performed in Patients 18 and 19 (Family 14). The *MADD* variant identified in Patients 4 and 21 was genotyped in the similarly affected sibling (Patients 3 and 22, respectively) by Sanger sequencing. Variant validation was performed by Sanger sequencing with DNA obtained from leucocytes and/or fibroblasts of patients and parents. Technical details and information on WGS/WES/Mendeliome, sequence data analysis, and validation and segregation of variants are described in the Supplementary material.

Copy number analysis

Real-time quantitative PCR on genomic DNA was performed as described previously (Moog *et al.*, 2011). Briefly, 30 ng DNA was used as template for SYBR® Green-based quantitative PCR (qPCR). The reaction was carried out using the Rotor Gene RG-3000 (Qiagen) and 2× SYBR® Green JumpStart™ Taq

ReadyMix™ (Sigma-Aldrich). The *CFTR* gene was used as an internal reference. Primer sequences are described in Supplementary Table 1. Relative quantification of exon copy numbers on genomic DNA was carried out using the comparative threshold cycle (ΔΔCT) method with Control 1 as calibrator. The relative exon copy number was calculated and was of ~2 for a diploid sample.

Transcript analysis

Total RNA was extracted (Monarch® Total RNA Miniprep Kit, New England Biolabs) from cultured primary fibroblasts. RNA concentration and purity of the samples were assessed by use of the Epoch™ Microplate Spectrophotometer (BioTek). Total RNA (1 μg) was reverse transcribed (LunaScript® RT SuperMix Kit, New England Biolabs). Reverse transcription (RT)-PCR fragments were generated according to standard PCR protocols with OneTaq® Quick-Load® 2× Master Mix (New England Biolabs). Primer sequences are described in Supplementary Table 1. PCR products were either directly Sanger-sequenced or cloned into pCR2.1 TOPO TA Cloning Vector (Thermo Fisher Scientific) according to manufacturer's instructions. *Escherichia coli* clones were subjected to colony PCR, and PCR products from individual clones were sequenced. A total of 93 and 189 clones were analysed for Patients 2 and 3, respectively.

For quantitative RT-PCR (RT-qPCR), technical duplicates of samples were prepared as a 10 μl approach with the SYBR® Green I-based Luna® Universal qPCR Master Mix (New England BioLabs), 500 nM of each primer, and 1 μl of cDNA. Primer sequences are described in Supplementary Table 1. RT-qPCR was performed using the QuantStudio™ 3 Real-Time PCR System (Thermo Fisher Scientific) equipped with QuantStudio™ Design & Analysis Software v1.4.3 (Thermo Fisher Scientific). The PCR conditions included a pre-run at 95°C for 5 min, followed by 40 cycles of 30 s at 95°C, 30 s at 58°C and 45 s at 72°C. PCR amplification specificity was determined by melting curve analysis with a range from 60°C to 95°C. The values of the cycle threshold (CT) of the target gene (*MADD*) were normalized to the housekeeping gene *GAPDH*. For relative gene expression the comparative cycle threshold (ΔΔCT) values were calculated with the QuantStudio™ Design & Analysis Software v1.4.3 with *GAPDH* as internal control and expressed as *x*-fold change to Control 1. Data analysis of multiple experiments was performed with the ExpressionSuite Software v1.3 (Thermo Fisher Scientific). Mean of technial duplicates from each experiment is shown in the Supplementary material.

Chemicals, antibodies and reagents

The following primary antibodies and dilutions were used for immunoblotting: rabbit polyclonal anti-p44/42 MAPK (ERK1/2) [1:1000; Cell Signaling Technology (CST); #9102]; rabbit polyclonal anti-phospho-p44/42 MAPK (ERK1/2) (Thr202/Tyr204) (1:1000; CST; #9101); rabbit monoclonal anti-MADD/DENN (1:500; clone EPR4919; Abcam; ab134117; recognizing the C-terminus of MADD); mouse monoclonal anti-Tubulin antibody (1:5000; clone DM1A; Sigma-Aldrich; #T9026).

The following secondary antibodies and dilutions were used for immunoblotting: goat anti-mouse IgG: StarBright Blue 700 antibody (1:10 000; #12004159; Bio-Rad); sheep anti-rabbit IgG: DyLight800 antibody (1:5000; #STAR36D800GA; Bio-Rad).

The following reagents were used: for induction of cellular stress and/or apoptosis, we used proteasome inhibitor MG-132 (Sigma-Aldrich), staurosporine (STS; Sigma-Aldrich), and recombinant human TNF-α (PeproTech) with cycloheximide (CHX; Sigma-Aldrich). For epidermal growth factor (EGF) internalization assay, we used Alexa Fluor™ 555-coupled EGF (Invitrogen; #E35350).

Cell culture

Primary fibroblasts obtained from a skin biopsy of Patients 2, 3, 6, 11 and 18, the mother of Patient 2 and two healthy individuals were cultured in Dulbecco's modified Eagle medium (DMEM; Thermo Fisher Scientific) supplemented with 10% foetal bovine serum (FBS; GE Healthcare) and penicillin-streptomycin (100 U/ml and 100 μg/ml, respectively; Thermo Fisher Scientific). Cells were tested for mycoplasma contamination by PCR and confirmed to be mycoplasma-free. Briefly, the supernatant of 2-day-old cultures was collected, boiled at 95°C for 5 min, and cell debris was removed by centrifugation (1 min at room temperature). The cleared medium (4 μl) was used in a standard PCR protocol with OneTaq® Quick-Load® 2× Master Mix (New England Biolabs). PCR products were separated by agarose gel electrophoresis. Primer sequences are described in Supplementary Table 1.

Immunoblot analysis

Patient and control fibroblasts were harvested in ice-cold RIPA buffer (50 mM Tris-HCl pH 8.0, 150 mM NaCl, 1% NP-40, 0.5% DOC, and 0.1% SDS) supplemented with Mini Protease Inhibitor and PhosSTOP™ (Roche) and lysed for 10 min on ice. Cell debris was removed by centrifugation for 10 min at 4°C, and 4× sample buffer (33% glycerol, 80 mM Tris-HCl pH 6.8, 0.3 M DTT, 6.7% SDS, 0.1% bromophenol blue) was added to the supernatant. Samples were boiled at 95°C for 5 min. Protein extracts were separated on SDS-PAGE under denaturing conditions and transferred to PVDF (polyvinylidene fluoride) membranes. Membranes were blocked with 5% non-fat dry milk or bovine serum albumin (BSA) in TBS-Tween followed by incubation with the indicated primary antibody at 4°C overnight and with fluorescent dye-linked secondary antibodies at room temperature for 1 h. Fluorescence signals were digitally imaged with a ChemiDoc MP (Bio-Rad). Band intensities were determined with the Image Lab v6.0 software (Bio-Rad). Uncropped blots are shown in the Supplementary material.

Epidermal growth factor phosphorylation

Fibroblasts were seeded into six-well plates (150 000 cells per well) and incubated in starvation medium (0.1% FBS/DMEM) overnight. Next day, cells were treated with 50 ng/ml TNF-α in starvation medium for 15 or 30 min or left untreated. Subsequently, plates were transferred on ice and rinsed with ice-cold phosphate-buffered saline (PBS). Cells were harvested in ice-cold RIPA buffer supplemented with Mini Protease Inhibitor and PhosSTOP™ (Roche), and lysates were subjected to SDS-

PAGE and immunoblot analysis. For quantification, pERK1/2 was normalized to total ERK1/2, and the ratio at 0 min was set to 1.

Measurement of caspase-3 and -7 activity

Fibroblasts were seeded into white flat-bottom 96-well microplates (5000 cells per well) and treated with 100 ng/ml TNF-α and 5 μg/ml CHX for 24 h, 1 μM STS for 24 h, 20 μM MG-132 for 16 h or left untreated under basal, steady state conditions. To determine caspase-3 and -7 activity, the Caspase-Glo® 3/7 Assay (Promega) was performed according to manufacturer's instructions. Luminescence signals were detected as relative light units with the Synergy™ H1 Hybrid Multi-Mode Reader (BioTek) using the Gen5 software v2.09 (BioTek). The signal ratio of treated to untreated cells was calculated.

FITC-annexin V/PE-propidium iodide apoptosis assay

Fibroblasts were seeded into six-well plates (150 000 cells per well) and treated with 100 ng/ml TNF-α and 5 μg/ml CHX for 24 h, 1 μM STS for 24 h, 20 μM MG-132 for 16 h or left untreated under basal, steady state conditions. After treatment, supernatant was transferred into a 5 ml flow cytometry tube. Cells were harvested via trypsinization, added to the flow cytometry tube and washed twice with PBS (300*g*, 5 min). For determination of early and late apoptotic cells, the FITC Annexin V Apoptosis Detection Kit I (BD Biosciences) was used according to the manufacturer's protocol, including FITC-Annexin V and PE-propidium iodide as staining reagents. Fluorescence signals were measured with the FACSCanto™ II (BD Biosciences) equipped with FACSDiva™ Software v.8.0.1 (BD Biosciences), and the open source Flowing Software 2.5.1 (http://flowingsoftware.btk.fi/index.php? page=1) was used for gating and analysis. The amount of early and late apoptotic cells under steady state conditions was subtracted from the amount of early and late apoptotic cells after treatment.

Epidermal growth factor internalization assay

Fibroblasts were plated into six-well plates (150 000 cells per well) and incubated under steady state conditions overnight. The next day, cells were serum-starved (0.1% FBS/DMEM) for 2 h followed by labelling with 1 μg/ml Alexa Fluor™ 555-coupled EGF in ice-cold starvation medium for 1 h at 4°C. Cells were rewarmed to 37°C in pre-warmed starvation medium for various times (0, 5, 10 and 15 min) to induce and follow internalization of EGF-Alexa Fluor™ 555. Subsequently, cells were transferred on ice, and remaining surface-bound EGF-Alexa Fluor™ 555 was removed by an acidic wash (0.2 M acetic acid, 0.5 M NaCl, pH 2.5) for 6 min. Cells were washed once in ice-cold PBS, twice in ice-cold starvation medium and once in PBS before trypsinization and fixation in 4% paraformaldehyde. After intensive washing, the median fluorescence intensity was measured with the LSRFortessa™ cell analyzer (BD Biosciences) equipped with FACSDiva™ Software v.8.0.1 (BD Biosciences), and the open source Flowing Software 2.5.1 was used for gating and analysis.

Data analysis and statistics

Quantitative data are presented by GraphPad Prism 8 software (Instat, GraphPad Software) as the mean ± standard deviation (SD). For MADD mRNA and protein amount quantification, measurement of caspase-3 and -7 activity and determination of the amount of apoptotic cells, statistical analysis via one-way ANOVA followed by a Bonferroni *post hoc* test for multiple comparisons was performed. For ERK1/2 phosphorylation and EGF internalization experiments, statistical analysis via two-way ANOVA followed by a Tukey *post hoc* test for multiple comparisons was performed. A P-value < 0.05 was considered statistically significant ($*P \leqslant 0.05$; $**P \leqslant 0.01$; $***P \leqslant 0.001$; $****P \leqslant 0.0001$).

Data availability

The authors declare that all data supporting the findings of this study are available within the paper and its Supplementary material. Consent restrictions preclude sharing of full datasets, and the consents do not cover the deposition of the next-generation sequencing data in a public database.

Results

Biallelic variants in *MADD* are associated with a pleiotropic disorder

We investigated two siblings of a non-consanguineous family (Family 1), a boy (Patient 1) and his sister (Patient 2), who presented with apnoea at birth, followed by repeated episodes of desaturation, muscular hypotonia, severe developmental delay, exocrine pancreatic insufficiency, growth hormone deficiency, and low haemoglobin. Patient 1 died at the age of 7.5 years; Patient 2 was 12 years old at last follow-up (Table 1). Both affected siblings were subjected to WES. Suspecting a Mendelian autosomal recessive trait, we observed that the siblings shared two rare, potentially pathogenic *MADD* variants in heterozygosity, c.914G > T/p.(Gly305Val) and an intragenic deletion of *MADD* exons 11 to 24 [c.(1862 + 1_1863-1)_(3759 + 1_3760-1)del; GenBank accession number: NM_003682.3] (Fig. 1, Table 1 and Supplementary Table 2). Both variants were absent in dbSNP138, 1000 Genomes Project, Exome Variant Server, and ExAC and gnomAD browsers (Table 1). By Sanger sequencing, we confirmed the *MADD* missense variant in the siblings and their mother in the heterozygous state (Supplementary Fig. 2A). The pathogenicity prediction algorithms CADD, REVEL and M-CAP predicted this amino acid substitution to have a damaging impact on protein function, and Gly305 was predicted to be intolerant to

Table 1 Biallelic *MADD* variants and key clinical features in 23 patients

Patient	Nucleotide change (NM_003682.3)	Amino acid alteration (NP_003673.3)	gnomAD browser: MAF [%]	Failure to thrive	DD and/or ID	Muscular hypotonia	Sensory and autonomic impairment	Endocrine abnormalities	Exocrine pancreatic insufficiency[a]	Early death
Group 1										
1 + 2[b]	c.914G>T	p.(Gly305Val)	Absent	+ / +	+ / +	+	+ / +	+	+ / +	7 y 5 m (Pt 1)
	c.(1862+1_1863-1)_(3759+1_3760-1)del	p.?[c]	Absent							
3[b] + 4	c.963+1G>A	p.?[c]	Absent	+ / +	+ / +	+	+ / +	+	+ / +	20 m (Pt 3)
5	c.979C>T	p.(Arg327*)	0.001989	+	+	+	+	+	+	16 m
	c.1705+1G>C	p.?	Absent							
6[b]	c.3119T>G	p.(Leu1040Arg)	Absent	+	+	+	+	+	–	15 m
7	c.646C>T	p.(Arg216*)	0.0004032	+	+	+	+	+	+	8 m
8	c.979C>T	p.(Arg327*)	0.001989	+	+	+	+	+	+	22 m
9	c.4293G>A	p.(Trp1431*)	Absent	+	+	+	+	+	+	Alive
10	c.979C>T	p.(Arg327*)	0.001989	+	+	+	+	ND	+	Alive
	c.3760-2A>C	p.?	Absent							
11[b]	c.770C>T	p.(Ser257Phe)	Absent	+	+	+	+	+	+	Alive
12	c.979C>T	p.(Arg327*)	0.001989	+	+	+	+	+	+	Alive
	c.4398delG	p.(Leu1467Cysfs*20)	Absent							
13 + 14	c.1115C>T	p.(Pro372Leu)	Absent	ND / +	+ / +	+ / +	+ / +	+ / +	+ / +	2 y 6 m (Pt 13)
	c.4080delG	p.(Lys1361Serfs*24)	Absent							
Group 2										
15	c.1037T>C	p.(Leu346Pro)	Absent	+	+	+	+	–	ND	Alive
16 + 17	c.3533_3534delCT	p.(Ser1178Cysfs*18)	Absent	– / –	+ / +	+ / +	+ / +	– / –	– / ND	Alive
	c.3848A>C	p.(Tyr1283Ser)	Absent							
18[b] + 19	c.1061C>T	p.(Pro354Leu)	0.001988	– / +	+ / +	– / –	– / –	– / –	– / –	Alive
	c.3637_3638delAG	p.(Ser1213*)	Absent							
20	c.3952T>C	p.(Trp1318Arg)	Absent	–	+	+	+	–	ND	3 y
21 + 22	c.2834T>C	p.(Leu945Pro)	Absent	– / –	+ / +	+ / –	+ / –	– / –	ND / ND	Alive
23	c.3637_3638delAG	p.(Ser1213*)	Absent	–	+	+	+	–	–	Alive
	c.4594C>T	p.(Arg1532*)	Absent							

[a]Exocrine pancreatic insufficiency has been determined by low level or absent faecal elastase-1

[b]Fibroblasts of the patient were used in functional studies.

[c]Detailed data of *MADD* mRNA analysis are shown in Fig. 2.

\+ = feature present; – = feature absent; DD = developmental delay; ID = intellectual disability; m = months; MAF = minor allele frequency; ND = no data; y = years. For siblings, the first plus or minus symbol refers to the clinical feature in the older sibling and the plus or minus symbol after the forward slash to the clinical feature in the younger sibling.

variation (Supplementary Table 2) (Kircher *et al.*, 2014; Ioannidis *et al.*, 2016; Jagadeesh *et al.*, 2016; Wiel *et al.*, 2019). Real-time qPCR of select *MADD* exons using genomic DNA confirmed one copy of the *MADD* exons 14, 20, and 23 in Patient 2 and her father, while the relative copy number of *MADD* exons 10 and 25 was comparable to a diploid sample in the two individuals (Supplementary Fig. 3). In fibroblast-derived cDNA of Patient 2, we identified predominant abundance of *MADD* transcripts with the c.914G>T variant suggesting nonsense-mediated mRNA decay (NMD) of transcripts harbouring the multi-exon deletion (Supplementary Fig. 2A). We analysed the effect of the *MADD* exon 11–24 deletion on mRNA level in fibroblasts of Patient 2. We characterized and determined the ratio of four different aberrant *MADD* transcripts harbouring a deletion or a deletion/insertion [r.1706_3759del (∼27%); r.[1706_3759del; 3868_3869ins3868+1_3868-1] (∼13%); r.1863_3759del (∼43%); r.[1863_3759del; 3868_3869ins3868+1_3868-1] (∼17%)], all leading to frameshift and premature stop codon [p.(Asn569Argfs*2) and p.(Ser621Argfs*7)] (Fig. 2A and B). Compound heterozygosity of a likely pathogenic missense and a loss-of-

function variant in *MADD* in the two affected siblings suggested that these alterations underlay their phenotype. This was further corroborated by a report on two unrelated individuals with developmental delay/expressive language delay carrying biallelic *MADD* variants (Anazi *et al.*, 2017) and the observation of only 44% of the expected *MADD* loss-of-function variants in the database gnomAD (observed/ expected score: 0.44).

We identified another family (Family 2) with two siblings (Patients 3 and 4) similarly affected as Patients 1 and 2 (Table 1). Patients 3 and 4 carry the homozygous splice site mutation c.963+1G>A in intron 4 of *MADD*, and parents were heterozygous (Fig. 1A, Table 1 and Supplementary Fig. 2B). By analysing fibroblast-derived cDNA of Patient 3, we found an in-frame deletion of the last 30 nucleotides of exon 4 in the majority of *MADD* transcripts [∼87%; r.934_963del/p.(Leu313_Val322del)]. The remaining identified *MADD* transcripts harboured an insertion of the first 7 bp of intron 4 (∼11%; r.963_964ins963+1_963+7) or a deletion of the last 50 nucleotides of exon 4 (∼2%; r.914_963del), both of which resulting in a frameshift and introduction of a premature stop codon
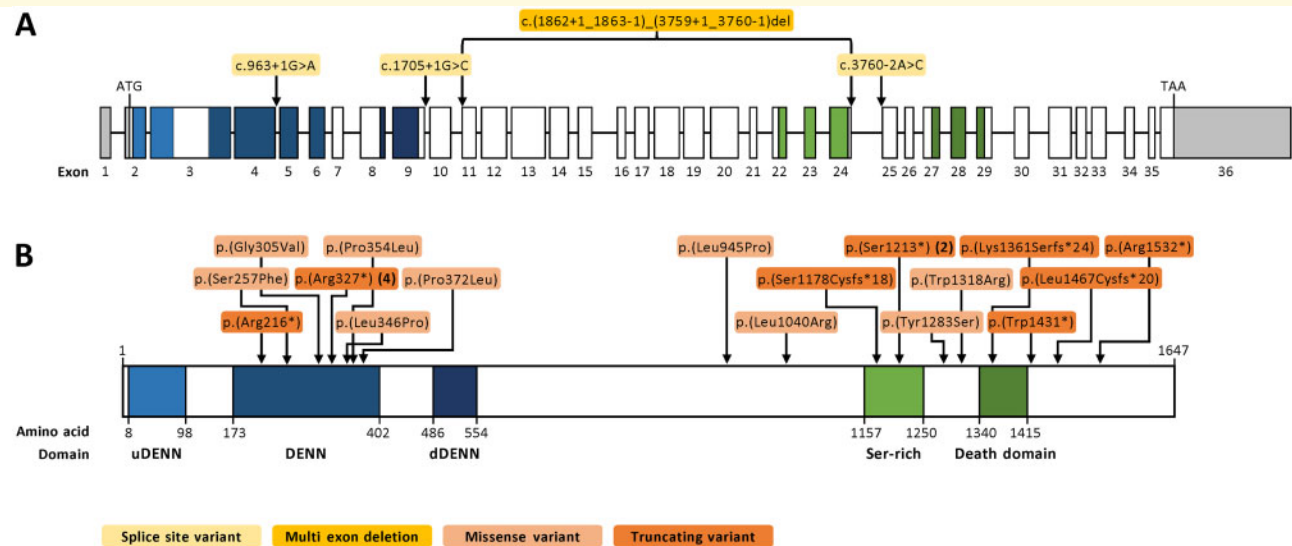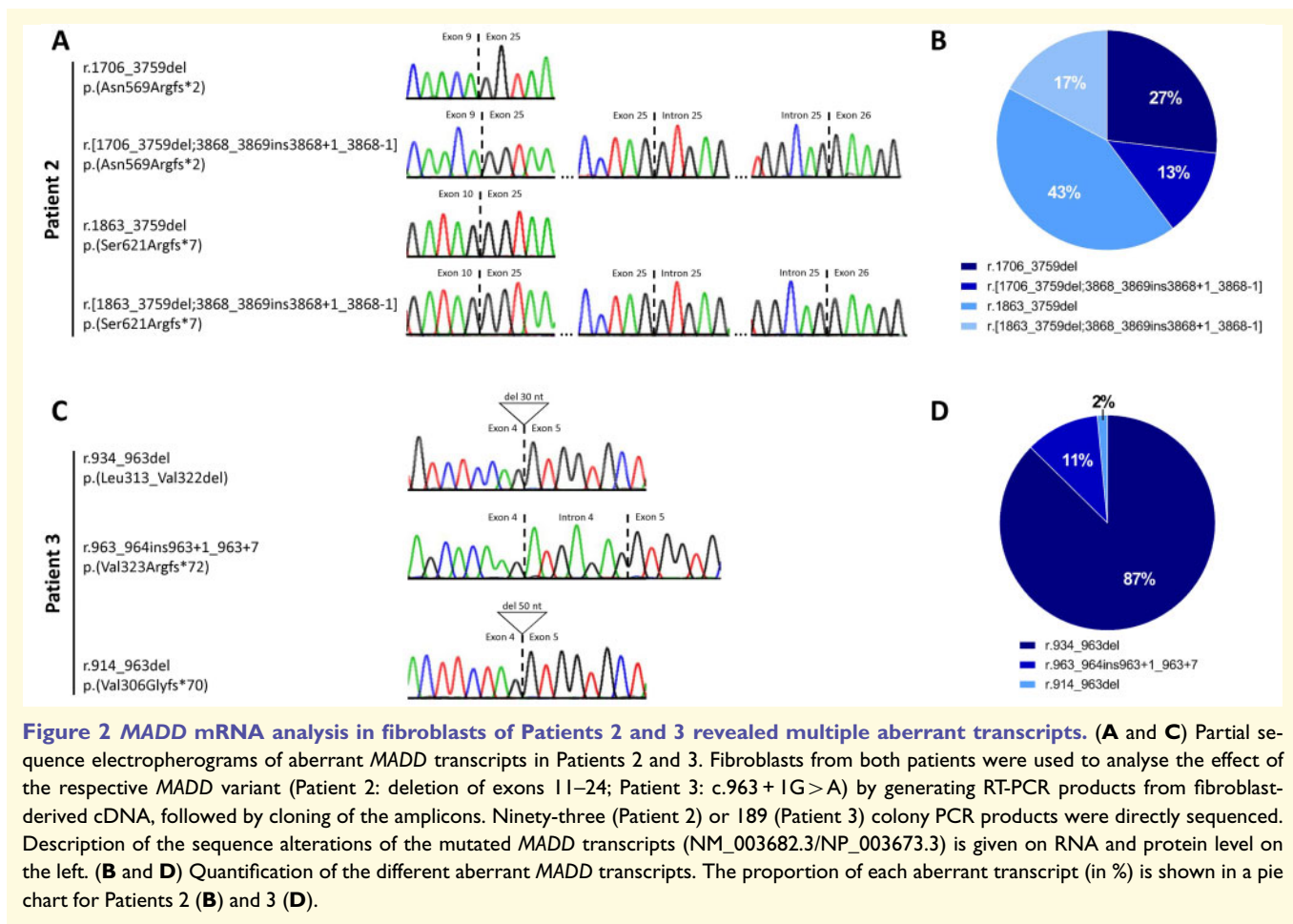
Figure 1 Schematic view of *MADD* exon-intron structure and protein domains with variants identified in 23 patients. (A)
Schematic overview of *MADD* exon-intron structure (NM_003682.3; not drawn to scale) showing the splice site variants (light yellow) found in
Patients 3 and 4 (c.963 + 1G > A), Patient 5 (c.1705 + 1G > C) and Patient 10 (c.3760-2A > C), and the deletion of exons 11 to 24 (dark yellow)
identified in Patients 1 and 2 [c.(1862 + 1_1863-1)_(3759 + 1_3760-1)del]. Exon numbers are given below the structure. 3′- and 5′-untranslated
regions are coloured in grey. Start codon is located in exon 2 and stop codon in exon 36. Exons coding for certain protein domains are coloured;
colours of respective protein domains are as follows: uDENN (light blue), DENN (mid blue), dDENN (dark blue), Ser-rich (light green) and
Death domain (dark green). Colours of the exons encoding domains in **A** match with colours of protein domains in **B**. (**B**) Schematic overview
of MADD protein structure (NP_003673.3) showing the missense variants (light orange) found in Patient 11 [p.(Ser257Phe)], Patients 1 and 2
[p.(Gly305Val)], Patient 15 [p.(Leu346Pro)], Patients 18 and 19 [p.(Pro354Leu)], Patients 13 and 14 [p.(Pro372Leu)], Patients 21 and 22
[p.(Leu945Pro)], Patient 6 [p.(Leu1040Arg)], Patients 16 and 17 [p.(Tyr1283Ser)], and Patient 20 [p.(Trp1318Arg)], and the truncating variants
(dark orange) found in Patient 7 [p.(Arg216*)], Patients 5, 8, 10 and 12 [p.(Arg327*)], Patients 16 and 17 [p.(Ser1178Cysfs*18)], Patients 18, 19
and 23 [p.(Ser1213*)], Patients 13 and 14 [p.(Lys1361Serfs*24)], Patient 9 [p.(Trp1431*)], Patient 12 [p.Leu1467Cysfs*20], and Patient 23
[p.(Arg1532*)]. The bold number in brackets indicates the number of unrelated individuals with this mutation. Amino acid positions and name of
protein domains are given below the structure.

[p.(Val306Glyfs*70) and p.(Val323Argfs*72)] (Fig. 2C and
D).

Through a national collaboration and GeneMatcher
(Sobreira *et al.*, 2015), we subsequently identified 19 add-
itional individuals with biallelic variants in *MADD*, bring-
ing the total number of patients with variants in this gene
to 23 (Table 1 and Supplementary Tables 3 and 4). Every
participating group/centre independently selected *MADD*
variants as the only potentially disease-causing variants
and did not consider other variants in known or candidate
genes as potentially disease-relevant. In total, we found 21
different rare variants in *MADD*, nine missense, five non-
sense, three splice, three frameshift, and one multi-exon de-
letion (Fig. 1, Table 1 and Supplementary Table 2). The 21
variants affect all seven different *MADD* transcript variants
(Supplementary Fig. 1). Patient 6 with the homozygous
missense variant c.3119T > G/p.(Leu1040Arg), confirmed
in DNA and cDNA of patient's fibroblasts (Supplementary
Fig. 2C), has already been reported, but without clinical
details and functional studies regarding the consequence of
the amino acid change (Anazi *et al.*, 2017). *MADD* var-
iants in Patients 11 and 18 were validated in fibroblast-

derived DNA and cDNA (Supplementary Fig. 2D and E).
Pathogenicity prediction algorithms predicted the nine
MADD missense variants to have a damaging impact on
protein function, and eight were absent in the gnomAD
browser (Table 1 and Supplementary Table 2). Five of nine
missense variants cluster in the central DENN domain,
while the remaining four missense variants are located in
the middle and C-terminal region of the protein, without
affecting any known domain (Fig. 1B). Six missense
changes affect an intolerant amino acid residue
(Supplementary Table 2). For the two intronic variants
c.1705 + 1G > C and c.3760-2A > C, both affecting a highly
conserved splice site, mRNA analysis could not be per-
formed, but splice site analysis tools predicted the variants
to have an impact on *MADD* pre-mRNA splicing
(Supplementary Table 2). In summary, based on rarity or
absence of the identified *MADD* variants in the population
databases, several truncating variants as well as missense
and splice variants with a predicted damaging effect, and
overlapping clinical features in the 23 affected individuals,
we were convinced that biallelic *MADD* variants underlie
the phenotype in all of them.

Figure 2 *MADD* mRNA analysis in fibroblasts of Patients 2 and 3 revealed multiple aberrant transcripts. (**A** and **C**) Partial sequence electropherograms of aberrant *MADD* transcripts in Patients 2 and 3. Fibroblasts from both patients were used to analyse the effect of the respective *MADD* variant (Patient 2: deletion of exons 11–24; Patient 3: c.963 + 1G > A) by generating RT-PCR products from fibroblast-derived cDNA, followed by cloning of the amplicons. Ninety-three (Patient 2) or 189 (Patient 3) colony PCR products were directly sequenced. Description of the sequence alterations of the mutated *MADD* transcripts (NM_003682.3/NP_003673.3) is given on RNA and protein level on the left. (**B** and **D**) Quantification of the different aberrant *MADD* transcripts. The proportion of each aberrant transcript (in %) is shown in a pie chart for Patients 2 (**B**) and 3 (**D**).

Biallelic *MADD* variants cause MADD deficiency or reduced MADD protein in five patient-derived fibroblast cell lines

To characterize the functional consequences of homozygous and compound heterozygous *MADD* variants, we used fibroblasts derived from Patients 2, 3, 6, 11 and 18. We first determined the relative *MADD* mRNA amount in the patient cells by RT-qPCR. *MADD* mRNA amount was reduced to ∼40% to ∼48% in fibroblasts of Patients 2, 3 and 18 compared to cells of Control 1 (set to 100%) (Fig. 3A). This can be explained by NMD of *MADD* transcripts harbouring a premature stop codon that are expressed from one or both *MADD* allele(s) in patient cells. In contrast, the *MADD* mRNA amount in cells of Patients 6 and 11 was comparable to that of control cells suggesting that transcripts with variants predicting amino acid substitutions are stable (Fig. 3A). Cells of the mother of Patient 2 had normal *MADD* mRNA level (Fig. 3A). We next used lysates of primary fibroblast cultures for MADD protein analysis via immunoblotting. The anti-MADD antibody was raised against a synthetic peptide

comprising part of the human MADD C-terminus and detects the ubiquitously expressed isoforms IG20-FL, MADD/DENN, IG20-SV2, IG20-SV3 and IG20. The isoforms IG20-SV4 and KIAA0385 will likely not be detected due to a different C-terminus (Supplementary Fig. 1); however, expression of these two MADD forms is restricted to neural tissues (Li *et al.*, 2008). MADD was almost completely absent in fibroblasts of Patients 2, 3, 11 and 18, while in cells of Patient 6 with the homozygous missense variant p.(Leu1040Arg) a small amount of mutant MADD was detectable (Fig. 3B). Relative quantification of the MADD protein confirmed significantly reduced levels in all patient cells, that was between 0% and 4% in fibroblasts of Patients 2, 3, 11 and 18 and ∼20% in Patient 6-derived cells in comparison to cells of Control 1 (Fig. 3C). In cells of the mother of patients 1 and 2, who was a healthy carrier of the heterozygous missense variant p.(Gly305Val), MADD protein level was reduced by ∼40% compared to Control 1 cells (Fig. 3B and C). The data show that biallelic *MADD* variants, including the missense variants p.(Ser257Phe), p.(Gly305Val), and p.(Leu1040Arg), lead to MADD deficiency or a drastic reduction in MADD protein amount in
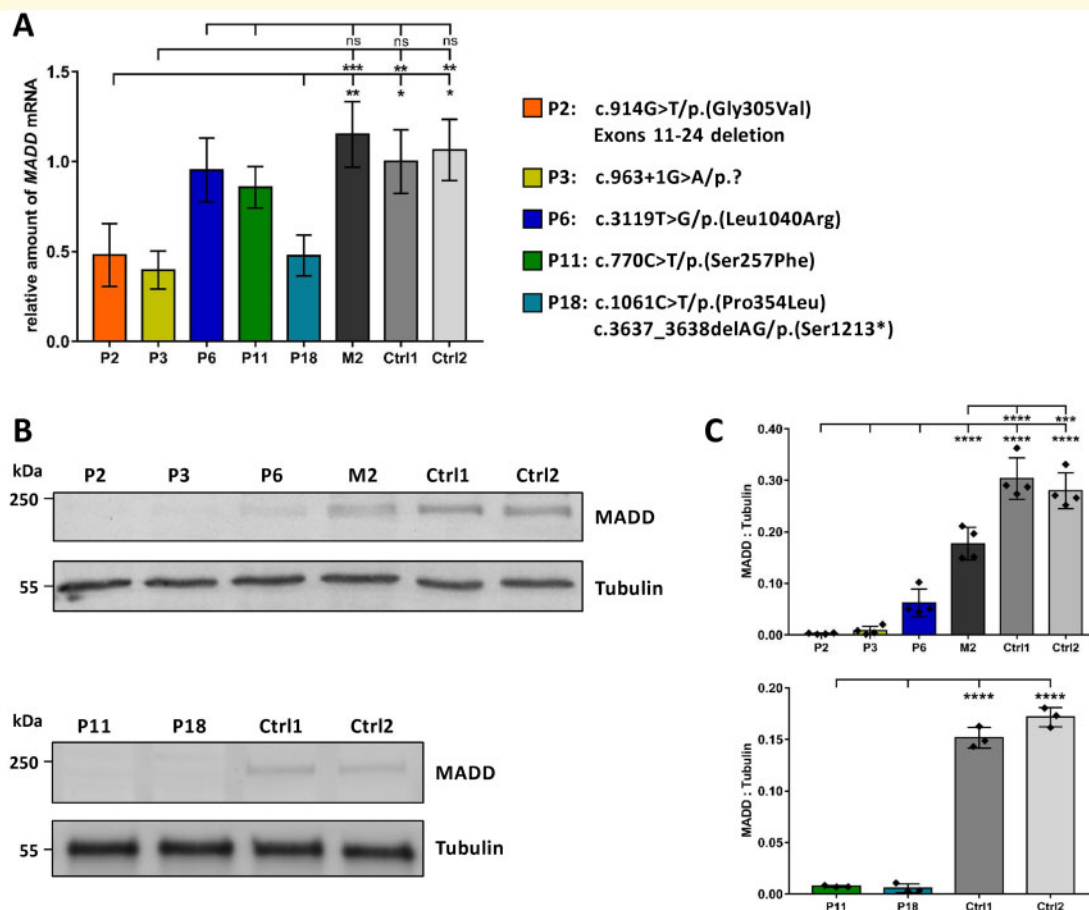
Figure 3 *MADD* **mRNA and protein amount is drastically reduced in fibroblasts of Patients 2, 3, 6, 11, and 18.** (**A**) Quantification of *MADD* transcripts by RT-qPCR. RNA was obtained from fibroblasts of Patients 2, 3, 6, 11 and 18, the mother of Patient 2 and two control subjects. The mean of three independent experiments ± SD is given. Mean of technial duplicates from each experiment is shown in the Supplementary material. One-way ANOVA with Bonferroni correction was used for statistical analysis. (**B**) Immunoblot of lysates obtained from fibroblasts of five patients, the mother of Patient 2 and two controls. The amount of MADD protein was monitored with an anti-MADD antibody, and an anti-tubulin antibody was used for equal loading. Uncropped blots are provided in the Supplementary material. (**C**) Band intensities of fluorescence signals were quantified using the ChemiDoc imaging system. The mean of three (Patients 11 and 18) or four (Patients 2, 3 and 6) independent experiments ± SD is given, and individual data-points from each experiment are shown. One-way ANOVA with Bonferroni correction was used for statistical analysis. *$P \leqslant 0.05$; **$P \leqslant 0.01$; ***$P \leqslant 0.001$; ****$P \leqslant 0.0001$. Ctrl 1 = Control 1; Ctrl 2 = Control 2; M2 = mother of Patient 2; P2 = Patient 2; P3 = Patient 3; P6 = Patient 6; P11 = Patient 11; P18 = Patient 18.

five patient fibroblast cell lines that is likely due to NMD of mutant transcripts and/or intrinsic instability or enhanced degradation of the produced protein.

The phenotype in patients with biallelic *MADD* variants ranges from developmental delay to a severe multisystem disorder

The 23 patients with biallelic *MADD* variants showed overlapping phenotypes as all had global developmental delay and/or intellectual disability, and the majority had muscular hypotonia and seizures (Table 1 and Supplementary Tables 3 and 4). However, we noticed major differences in the

phenotypes of the 23 patients. Fourteen had a complex clinical picture and came to medical attention during the perinatal period with respiratory distress, apnoea, severe muscular hypotonia, and/or hypoglycaemia. The course of disease in the 14 patients, forming patient Group 1 (Table 2 and Supplementary Table 3), was characterized by dysfunction of multiple organ systems. Repeated episodes of apnoea and/or desaturation were observed in 13 patients, which started in the neonatal period and improved over time. Temperature dysregulation and/or intermittent or constant fever were reported in 11 individuals, and diarrhoea and/or obstipation in 13. Reduced sweating was observed in six patients, reduced pain sensation in nine, crying without tears in five and self-mutilation in six patients. These features are characteristic of sensory and autonomic dysregulation.
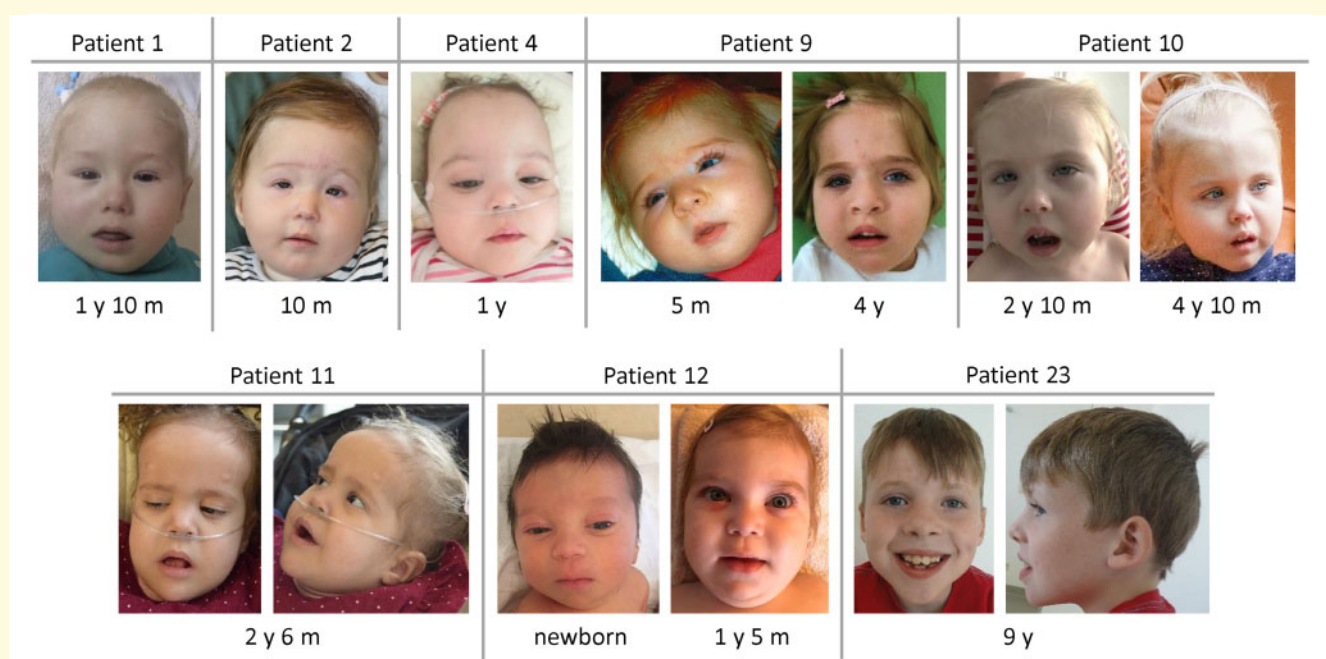
Figure 4 Facial photographs of eight patients with biallelic *MADD* variants. Patients 1, 2, 4, 9, 10, 11 and 12 showed the severe multi-systemic phenotype (Group 1), while Patient 23 had the predominant neurological phenotype (Group 2). All patients with the pleiotropic disorder had a myopathic facial expression with open mouth, high or broad forehead, depressed or wide nasal bridge, short nose, and small mouth with tented upper lip vermilion. Patients 1, 2 and 9 had small palpebral fissures that were more pronounced in infancy. The philtrum was short in Patients 10 and 11. The two skin lesions on the temporal forehead of Patient 11 resulted from non-invasive ventilation device in her previous treatments. The mildly affected Patient 23 had minor facial dysmorphism with wide nasal bridge, low hanging columella, and low-set, posteriorly rotated ears.

Other constant findings were exocrine pancreatic insufficiency (low level or absent faecal elastase-1) in 13 individuals and endocrine dysfunction, characterized by hypothyroidism in six patients, and growth hormone deficiency and (pan)hypopituitarism in eight each. Repeated hypoglycaemia was observed in 12 individuals, insufficient weight gain in 10, and postnatal growth retardation in 13. An abnormal pituitary gland was detected in brain MRI of two patients. Haematological abnormalities comprised low haemoglobin in 13 patients and thrombocytopenia in five. The overall outcome in patient Group 1 was poor: six patients died before their third year of life, and one child at the age of 7.5 years.

The other nine patients had mild-to-severe developmental delay and/or intellectual disability as common features and formed patient Group 2 (Table 2 and Supplementary Table 4). Motor and speech developmental delay or impairment was found in seven individuals, and muscular hypotonia and seizures in six patients each. Characteristic features of the pleiotropic disorder of Group 1 patients, such as postnatal failure to thrive, repeated episodes of apnoea and/or desaturation, reduced pain sensation and obstipation and/or diarrhoea were observed only in a few of the nine affected individuals, and temperature dysregulation, reduced sweating, and exocrine and endocrine dysfunction in none of them.

Craniofacial dysmorphism was present in almost all of the 23 patients (Fig. 4 and Supplementary Tables 3 and 4). In particular, full cheeks, small mouth and tented upper lip were frequent dysmorphic features in infants; however, we did not observe a common and recognizable facial gestalt in the eight individuals shown in Fig. 4.

Reduced TNF-α-dependent activation of the MAP kinases ERK1/2 in patient-derived fibroblasts

MADD is required for TNF-α-mediated activation of the MAPK pathway, including ERK1/2, in several cell lines (Schievella *et al.*, 1997; Murakami-Mori *et al.*, 1999; Al-Zoubi *et al.*, 2001; Kurada *et al.*, 2009). In *MADD* knockdown cells, TNF-α treatment did not induce phosphorylation of ERK1/2 (Kurada *et al.*, 2009). We next determined the phosphorylation status of ERK1/2 in serum-starved fibroblasts that were treated with TNF-α. We identified an increase over baseline in ERK1/2 phosphorylation after 15 min and 30 min of TNF-α treatment for both the patient and control cells (Fig. 5A). However, the responses to TNF-α were significantly less in patient cells (Fig. 5A). ERK1/2 phosphorylation after 15 min of TNF-α treatment

Table 2 Main clinical characteristics of 23 patients with biallelic *MADD* variants

Clinical feature	Number of patients	
	14 (Group 1)	9 (Group 2)
Impairment of neurological function		
Developmental delay	14 / 14	9 / 9
Impaired/delayed motor development	14 / 14	7 / 8
Impaired/delayed speech development	9 / 11	7 / 8
Intellectual disability	3 / 3	5 / 5
Muscular hypotonia	14 / 14	6 / 9
Seizures	9 / 14	6 / 9
Abnormal EEG	9 / 13	6 / 7
Impairment of sensory and autonomic system		
Obstipation and/or diarrhoea	13 / 14	3 / 7
Repeated episodes of apnoea and/or desaturations	13 / 14	3 / 9
Temperature dysregulation/fever of unknown origin	11 / 13	0 / 7
Reduced sweating	6 / 11	0 / 8
Reduced pain sensation	9 / 12	2 / 8
Self-mutilation	6 / 11	1 / 8
Crying without tears	5 / 13	1 / 8
Exocrine and endocrine dysfunction		
Exocrine pancreatic insufficiency	13 / 14	0 / 4
Growth hormone deficiency	8 / 10	0 / 5
Hypothyroidism	6 / 13	0 / 8
(Pan)hypopituitarism	8 / 12	0 / 5
Hypoglycaemia	12 / 13	0 / 7
Postnatal failure to thrive		
Low weight ($<-2.0z$)	10 / 13	2 / 9
Low length/height ($<-2.0z$)	13 / 13	1 / 7
Haematological abnormalities		
Low haemoglobin	13 / 14	3 / 9
Thrombocytopenia	5 / 14	1 / 8

z = z-score.

was 1.9–2.3-fold lower in cells from Patients 2, 3, 6, 11 and 18 than in Control 1 fibroblasts (Fig. 5B). Similarly, after 30 min of TNF-α treatment, the phosphorylation level of ERK1/2 was significantly reduced by 1.9–2.6-fold in the five patient-derived cell lines compared to Control 1 cells (Fig. 5B). Together, these data demonstrate that TNF-α-induced activation of the MAPK signalling pathway was suppressed in MADD-deficient patient cells that is in line with the requirement of MADD for TNFR1-mediated activation of MAP kinases (Kurada *et al.*, 2009).

MADD deficiency triggers TNF-α-dependent apoptosis

MADD was found to be overexpressed in many types of human tumours and tumour cell lines, where it contributes to resistance of cancer cells to TNF-α-induced apoptosis (Chow and Lee, 1996; Efimova *et al.*, 2004; Turner *et al.*, 2013). Accordingly, knockdown of endogenous MADD makes cells susceptible to TNF-α-induced apoptosis (Mulherkar *et al.*, 2006; Li *et al.*, 2008; Kurada *et al.*, 2009). To see if a similar effect was present in patient-derived cells, we treated fibroblasts of five patients and three control subjects with TNF-α and CHX or cultured them under normal conditions and monitored the activation status of the effector caspases 3 and 7 that execute cell death. TNF-α treatment of fibroblasts caused a higher activation of the two caspases in patient than in control cells, i.e. caspase-3 and -7 activity was 1.4–1.9-fold higher in the five patient-derived cell lines than in Control 1 cells (Fig. 5C). Treatment of patient cells with STS and MG-132, which both activate the intrinsic apoptosis pathway (Caballero-Benitez and Moran, 2003; McKenna *et al.*, 2010), induced a similarly elevated activation of caspase-3 and -7 in patient compared to control cells (by 1.8–3.2- and 1.9–3.9-fold, respectively) (Supplementary Fig. 4). Our data demonstrate enhanced susceptibility of patient-derived fibroblasts with MADD deficiency to TNF-α, but also other cellular stressors, that resulted in activation of the intrinsic apoptosis pathway and possibly increased cell death.

We next determined the amount of early and late apoptotic cells after treatment of fibroblasts with TNF-α and CHX and found a striking increase in the percentage of early and late apoptotic cells in MADD-deficient cells compared to control cells (Fig. 5D and E). TNF-α treatment caused a highly significant increase in the percentage of early apoptotic cells by 43–52.7-fold in three patient cell lines compared to Control 1 cells (Fig. 5D). While TNF-α treatment had an anti-apoptotic effect in control cells, as we observed 0.5–1% fewer late apoptotic cells in treated compared to untreated control cells, 1–1.4% of patient cells were late apoptotic after TNF-α treatment compared to untreated patient cells (Fig. 5E). Similarly, STS or MG-132 treatment induced a significant increase in the amount of early and late apoptotic cells in patient compared with control cells (Supplementary Fig. 5). These data confirm increased sensitivity of MADD-deficient cells to stressors promoting activation of the intrinsic apoptosis pathway.

MADD-deficient fibroblasts show decreased epidermal growth factor internalization

By acting as a guanine nucleotide exchange factor (GEF), MADD activates the small GTPases Rab3 and Rab27 (Wada *et al.*, 1997; Figueiredo *et al.*, 2008; Yoshimura *et al.*, 2010). Active Rab proteins promote membrane trafficking events, such as vesicle budding from donor membranes, vesicle transport and docking and fusion of the transport vesicle with acceptor membranes (Stenmark, 2009). MADD is not only required for synaptic exocytosis in neurons and granule exocytosis in parotid acinar cells (Tanaka *et al.*, 2001; Yamaguchi *et al.*, 2002; Imai *et al.*, 2013), but also for axonal transport of Rab3-carrying vesicles (Niwa *et al.*, 2008), suggesting a more general role of MADD in intracellular trafficking events. Therefore, we studied the effect of MADD deficiency on EGF
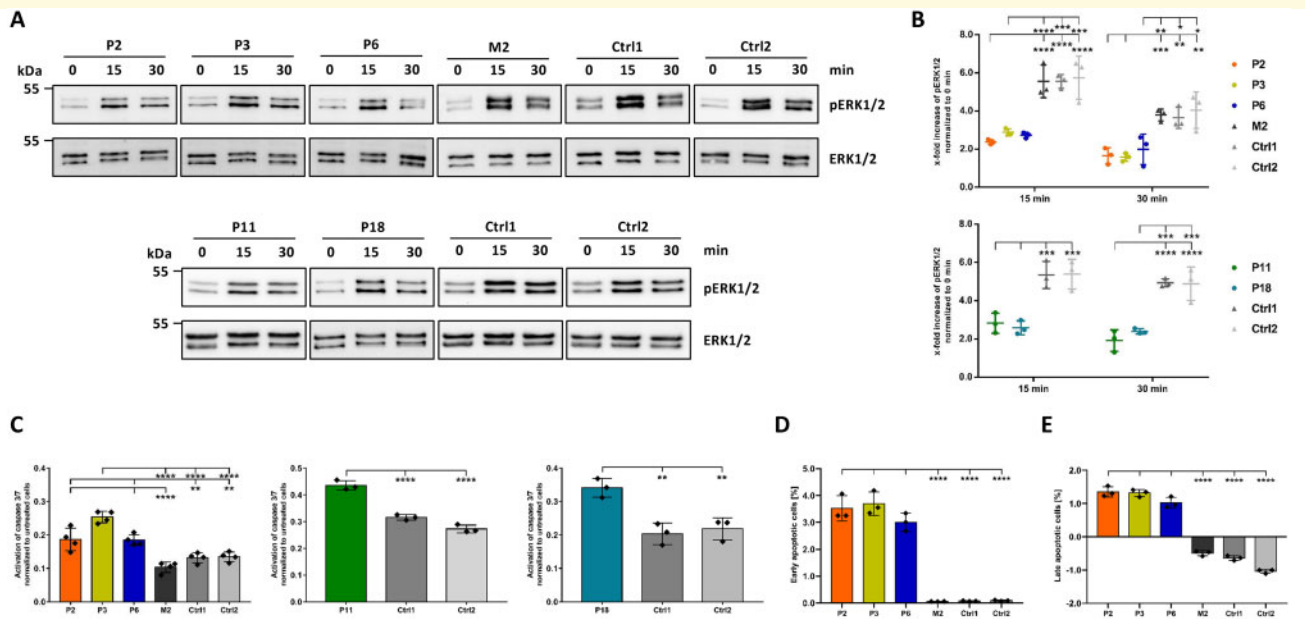
Figure 5 Effects of TNF-α treatment on ERK1/2 activation and cell death in patient-derived fibroblasts. (A) Immunoblot of lysates obtained from fibroblasts of Patients 2, 3, 6, 11 and 18, the mother of Patient 2 and two control subjects. After serum starvation overnight, cells were incubated in medium containing 50 ng/ml TNF-α for the indicated times. Cell lysates were analysed for the detection of endogenous phosphorylated ERK1/2 (pERK1/2) and total ERK1/2 by immunoblotting. Representative blots are shown. Uncropped blots are provided in the Supplementary material. **(B)** Band intensities of fluorescence signals were quantified using the ChemiDoc™ imaging system. pERK1/2 was normalized to total ERK1/2, and the ratio at 0 min was set to 1. The mean of three independent experiments ± SD is given, and individual datapoints from each experiment are shown. Two-way ANOVA with Tukey correction was used for statistical analysis. **(C)** Fibroblasts were treated with 100 ng/ml TNF-α and 5 μg/ml CHX for 24 h or left untreated. Activation of caspase-3 and -7 was determined by the Caspase-Glo® 3/7 assay according to the manufacturer's instructions. Luminescence signals were detected as relative light units by luminometer. The signal ratio of treated to untreated cells is given. The mean of four (left) or three (middle and right) independent experiments ± SD is given, and individual datapoints from each experiment are shown. One-way ANOVA with Bonferroni correction was used for statistical analysis. **(D and E)** Fibroblasts were treated with 100 ng/ml TNF-α and 5 μg/ml CHX for 24 h or left untreated. Proportion of apoptotic cells was measured with the Apoptosis Detection Kit according to the manufacturer's instructions. Cells were analysed by flow cytometry. Annexin V-positive cells are early apoptotic **(D)** and Annexin V-propidium iodide double-positive cells are late apoptotic **(E)**. The proportion of apoptotic cells in untreated samples was subtracted from the proportion of apoptotic cells in treated samples. Percentage of early and late apoptotic cells is shown. The bars and errors represent the mean ± SD of three independent experiments, and individual datapoints from each experiment are shown. One-way ANOVA with Bonferroni correction was used for statistical analysis. *$P \leqslant 0.05$; **$P \leqslant 0.01$; ***$P \leqslant 0.001$; ****$P \leqslant 0.0001$. Ctrl 1 = Control 1; Ctrl 2 = Control 2; M2 = mother of Patient 2; P2 = Patient 2; P3 = Patient 3; P6 = Patient 6; P11 = Patient 11; P18 = Patient 18.

internalization by measuring the internalized amount of fluorescently labelled EGF over a 15-min time course. After 10 and 15 min, we found a significant reduction in the amount of internalized EGF by 16–26% and 12–25%, respectively, in MADD-deficient cells of Patients 2, 3, 6, 11 and 18 compared to Control 1 cells (Fig. 6).

Discussion

We show here that biallelic *MADD* variants cause a neurodevelopmental disorder with and without numerous manifestations in multiple organs. On one end of the spectrum, mild developmental delay with absence epilepsy was present in a 19-year-old female (Patient 18 in Group 2). On the other end of the spectrum, we defined the core phenotype of a severe pleiotropic disorder in 14 individuals (Patients 1–

14; Group 1) that comprises the key abnormalities of severe developmental delay, hypotonia, sensory and autonomic neuropathy, endocrine and exocrine dysfunction, and haematological anomalies. The clinical course during the first years of life can be severe and potentially fatal. In MADD-deficient fibroblasts, we found several TNF-α-stimulated pathways to be disturbed. TNF-α treatment of patient cells resulted in decreased activation of the MAP kinases ERK1/2 and increased activation of the intrinsic apoptosis pathway. Reduced endocytosis of EGF in patient cells suggests a possible link between vesicle trafficking defect and impaired exocytosis. Based on our data, we assume that disruption of the manifold MADD functions may underlie the different clinical sub-phenotypes in the patient cohort with the multisystemic disorder. For example, decreased endocrine and exocrine secretion activity in the patients may be related to defects in exocytosis caused by diminished Rab3 and Rab27
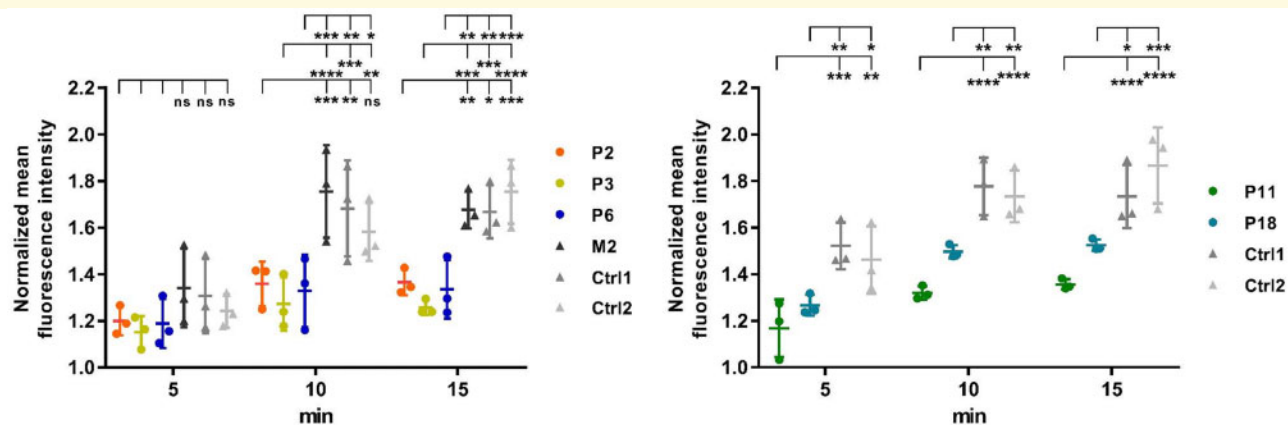
Figure 6 MADD loss leads to decreased EGF internalization in patient-derived fibroblasts. After serum starvation, fibroblasts were incubated with Alexa Fluor 555-coupled EGF and rewarmed for the indicated times. Surface-attached EGF-Alexa Fluor 555 was removed by an acidic wash. The amount of internalized EGF-Alexa Fluor 555 was determined by flow cytometry. The bars and errors represent the mean ± SD of the mean fluorescence intensity normalized to time-point 0 min of three independent experiments, and individual datapoints from each experiment are shown. Two-way ANOVA with Tukey correction was used for statistical analysis: $*P \leqslant 0.05$; $**P \leqslant 0.01$; $***P \leqslant 0.001$; $****P \leqslant 0.0001$. Ctrl 1 = Control 1; Ctrl 2 = Control 2; M2 = mother of Patient 2; ns = not significant; P2 = Patient 2; P3 = Patient 3; P6 = Patient 6; P11 = Patient 11; P18 = Patient 18.

activity, while the neuropathy may develop due to trafficking defects of Rab3-positive vesicles to nerve terminals.

The core clinical features of the severe pleiotropic disorder we describe here show considerable overlap with the infantile-onset multisystem neurological, endocrine, and pancreatic disease (IMNEPD; OMIM: 616263) that is caused by biallelic *PTRH2* variants (Hu *et al.*, 2014). A total of 14 individuals with homozygous *PTRH2* mutations, comprising the frameshift variant c.269_270delCT/p.(Ala90Glyfs*13), the nonsense variant c.324G > A/p.(Trp108*), and the missense variant c.254A > C/p.(Gln85Pro), and variable phenotypes have been reported (Hu *et al.*, 2014; Alazami *et al.*, 2015; Picker-Minh *et al.*, 2016; Sharkia *et al.*, 2017; Le *et al.*, 2019). The core features of IMNEPD include intellectual disability, motor and speech delay, ataxia, sensorineural hearing loss, and pancreatic insufficiency, while progressive cerebellar atrophy, peripheral neuropathy, hypothyroidism, hepatomegaly and/or abnormal liver parenchyma morphology have occasionally been observed in affected individuals (Picker-Minh *et al.*, 2016). At the mild end of the spectrum, sensorimotor peripheral neuropathy and sensorineural hearing loss have been reported in three sisters with the homozygous p.(Gln85Pro) mutation (Sharkia *et al.*, 2017). As patients with *PTRH2* loss-of-function mutations tended to have a more severe phenotype than those with the amino acid change p.(Gln85Pro), a possible genotype-phenotype correlation has been postulated (Picker-Minh *et al.*, 2016; Sharkia *et al.*, 2017; Le *et al.*, 2019). Similar to MADD, PTHR2 (also known as Bcl-2 inhibitor of transcription) is a multifunctional protein that participates in a variety of cellular functions, such as cell death and survival and protein synthesis in mitochondria (De Pereda *et al.*, 2004; Jan *et al.*, 2004; Kairouz-Wahbe *et al.*, 2008; Griffiths *et al.*,

2011). The neonatal diabetes mellitus with congenital hypothyroidism (NDH) syndrome (OMIM: 610199), characterized by intrauterine growth retardation, early onset of non-immune diabetes mellitus and congenital hypothyroidism, also shows partial phenotypic overlap with the pleiotropic disorder reported here. Biallelic pathogenic variants in the *GLIS3* gene have been reported in 13 patients with NDH syndrome (Senee *et al.*, 2006; Dimitri *et al.*, 2011, 2015; Alghamdi *et al.*, 2017). Besides the cardinal features, additional manifestations comprise facial dysmorphism, developmental delay and learning difficulties, sensorineural hearing loss, renal parenchymal disease, hepatic disease, exocrine pancreatic dysfunction, and skeletal and genital abnormalities (Dimitri *et al.*, 2015; Alghamdi *et al.*, 2017). GLIS3 belongs to a subfamily of Krüppel-like zinc finger proteins, functions as activator or repressor of gene transcription, and plays a critical role in the regulation of multiple biological processes (Jetten, 2018). Variability in the phenotype has been attributed to the differential expression of multiple *GLIS3* transcripts and the type of mutation (Senee *et al.*, 2006; Dimitri *et al.*, 2015).

The predominant neurological phenotype in 9 of 23 affected individuals with biallelic *MADD* variants (Patients 15–23; Group 2) comprises mild-to-severe developmental delay and/or intellectual disability, hypotonia, speech impairment, and seizures. Clinical hallmarks of the multisystem disorder, such as features of sensory and autonomic neuropathy, gastrointestinal anomalies, endocrine and exocrine dysfunction, and haematological anomalies were rarely reported or even absent in the nine individuals (Tables 1 and 2). *MADD* variants in the nine patients affect all *MADD* transcript variants, similar to the variants identified in the 14 more severely affected individuals (Supplementary Fig.

1). A genotype-phenotype correlation could not be established. For example, both Patient 9 with multisystemic disorder in Group 1 and Patient 23 with moderate global developmental delay in Group 2 had biallelic loss-of-function variants. A homozygous missense variant was found in Patient 11 in Group 1 and Patient 15 in Group 2. In addition, individuals with relatively mild (e.g. Patients 18 and 19 in Group 2) and severe clinical manifestations (e.g. Patients 1 and 2 in Group 1) carried a heterozygous truncating variant in *trans* with a heterozygous missense variant. Three previously reported patients with compound heterozygous *MADD* missense and nonsense variants were also mildly affected as one had expressive language delay, autism and poor eye contact (Anazi *et al.*, 2017), and two adult siblings had macrocephaly and mild-to-moderate intellectual disability (Hu *et al.*, 2019). Genital abnormalities, such as small penis and undescended testes, can be found in male individuals of both patient groups (8 of 12 males). In the caspase activity assay, fibroblasts derived from the mildly affected Patient 18 behave like those of the other patients. As most individuals described here have unique variants, and the effect of all variants has not been studied, we cannot exclude a yet-to-be-defined genotype-phenotype correlation. However, additional genetic, epigenetic and/or environmental factors may contribute to the clinical outcome in individuals with biallelic *MADD* variants, and the associated clinical spectrum is wide, with neurological manifestations at one end and early fatal outcome at the other end.

MADD has been proposed to protect neurons from cell death under conditions of cytotoxic stress, because MADD protein was reduced in the hippocampus in areas of Alzheimer's disease pathology, and antisense silencing of *MADD* promoted death of cultured rat hippocampal neurons (Del Villar and Miller, 2004). Thus, by acting as pro-survival factor MADD may prevent stress-induced cell death, especially upon physiological TNF-α activation. This suggests that MADD deficiency makes cells susceptible to TNF-α-induced apoptosis that may be followed by neurodegenerative or other degenerative processes in the patients.

MADD activates the Rab3 family and Rab27A and B (Wada *et al.*, 1997; Yoshimura *et al.*, 2010). The isoforms Rab3A–D are involved in exocytosis of synaptic vesicles and regulated secretory granules (Lang and Jahn, 2008). Analysis of *Madd* knockout animals revealed this Rab3 GEF to be implicated in the formation and trafficking of synaptic vesicles for regulated exocytosis (Tanaka *et al.*, 2001; Bae *et al.*, 2016). Madd also acts as Rab3 effector by binding GTP-bound Rab3 and transporting Rab3-carrying vesicles along axons through interaction with the motor proteins KIF1Bβ and KIF1A (Niwa *et al.*, 2008). Inhibition of Rab3-mediated exocytosis in *Madd* knockout mice has been hypothesized to cause a delay in endocytosis (Tanaka *et al.*, 2001). Thus, impaired endocytosis of EGF in MADD-deficient fibroblasts may provide a link to defective exocytosis in these and other cell types of the patients. Similar to the manner in which FAM45A, another DENN domain-containing protein, regulates the late endocytic pathway, including endocytosis and endosomal secretion (Zhang *et al.*, 2019), MADD could be a regulator of late/multivesicular endosomal trafficking.

Rab27A and Rab27B are expressed in various secretory cells, including endocrine, exocrine and immune cells and are involved in the regulated secretion of lysosome-related organelles and secretory granules (Gomi *et al.*, 2007; Fukuda, 2013). In particular, the two Rab proteins regulate exocytosis in pancreatic and lacrimal gland acinar cells, amylase release from parotid acinar cells, and granule secretion in mast cells and platelets (Chen *et al.*, 2004; Imai *et al.*, 2004; Gomi *et al.*, 2007; Mizuno *et al.*, 2007; Tolmachova *et al.*, 2007; Chiang *et al.*, 2011). Interestingly, by exchanging GDP for GTP in Rab27, MADD functions in isoproterenol-stimulated amylase release from rat parotid acinar cells (Imai *et al.*, 2013), and the GTPases Rab27A, Rab27B and Rab3 work in the exocytic machinery of the pituitary gland (Zhao *et al.*, 2002; Gomi *et al.*, 2007; Matsuno *et al.*, 2011). Thus, the function of Rab3 and Rab27 family members in special types of secretion remarkably overlaps with the dysfunction of endocrine and exocrine glands observed in Group 1 of individuals with MADD deficiency. For example, growth hormone deficiency, hypothyroidism, (pan)hypopituitarism and exocrine pancreatic insufficiency may be related to decreased endocrine and exocrine secretion activity in the patients. In contrast, other clinical features, such as repeated episodes of apnoea and/or desaturation in the neonatal period are unlikely to be attributed to defects in secretory pathways. This assumption is corroborated by the viability of *Rab27a/b* double knockout mice (Gomi *et al.*, 2007), which contrasts with the death of *Madd* knockout mice immediately after birth (Tanaka *et al.*, 2001). MADD has been implicated in neonatal survival as MADD-deficient newborn mice developed normally but had respiratory problems in the neonatal period (Tanaka *et al.*, 2001), similar to Group 1 patients with pathogenic *MADD* variants. Newborn knockout mice of *Kif1b*, encoding a MADD interaction partner, also die due to apnoea, and *Kif1b*^{+/−} mice have a defect in transport of synaptic vesicle precursors causing peripheral neuropathy (Zhao *et al.*, 2001). MADD also interacts with KIF1A, another motor protein, mediating axonal transport of Rab3-positive vesicles (Niwa *et al.*, 2008), and biallelic variants in this gene underlie hereditary sensory and autonomic neuropathy (HSAN) type II (Riviere *et al.*, 2011). These observations, together with defective neuromuscular transmission in Madd-deficient mice (Tanaka *et al.*, 2001), reinforce the presence of HSAN-typical features in Group 1 patients with *MADD* variants, such as reduced pain sensitivity, elevated body temperature, recurrent episodes of fever, repeated episodes of apnoea and/or desaturation, and intestinal dysmotility.

In summary, our study provides evidence that MADD is crucial for coordinating exocrine, endocrine, and neurological functions. Its functional loss causes a human disorder with a wide phenotypic spectrum ranging from predominant neurological abnormalities to a recognizable multisystem

condition comprising a characteristic constellation of neurological, endo- and exocrinological, and haematological findings.

Competing interests

The authors report no competing interests.

Supplementary material

Supplementary material is available at *Brain* online.

Appendix 1

The Undiagnosed Diseases Network consists of the following members:

Maria T. Acosta; Margaret Adam; David R. Adams; Pankaj B. Agrawal; Mercedes E. Alejandro; Justin Alvey; Laura Amendola; Ashley Andrews; Euan A. Ashley; Mahshid S. Azamian; Carlos A. Bacino; Guney Bademci; Eva Baker; Ashok Balasubramanyam; Dustin Baldridge; Jim Bale; Michael Bamshad; Deborah Barbouth; Gabriel F. Batzli; Pinar Bayrak-Toydemir; Anita Beck; Alan H. Beggs; Edward Behrens; Gill Bejerano; Jimmy Bennet; Beverly Berg-Rood; Raphael Bernier; Jonathan A. Bernstein; Gerard T. Berry; Anna Bican; Stephanie Bivona; Elizabeth Blue; John Bohnsack; Carsten Bonnenmann; Devon Bonner; Lorenzo Botto; Brenna Boyd; Lauren C. Briere; Elly Brokamp; Gabrielle Brown; Elizabeth A. Burke; Lindsay C. Burrage; Manish J. Butte; Peter Byers; William E. Byrd; John Carey; Olveen Carrasquillo; Ta Chen Peter Chang; Sirisak Chanprasert; Hsiao-Tuan Chao; Gary D. Clark; Terra R. Coakley; Laurel A. Cobban; Joy D. Cogan; F. Sessions Cole; Heather A. Colley; Cynthia M. Cooper; Heidi Cope; William J. Craigen; Andrew B. Crouse; Michael Cunningham; Precilla D'Souza; Hongzheng Dai; Surendra Dasari; Mariska Davids; Jyoti G. Dayal; Matthew Deardorff; Esteban C. Dell'Angelica; Shweta U. Dhar; Katrina Dipple; Daniel Doherty; Naghmeh Dorrani; Emilie D. Douine; David D. Draper; Laura Duncan; Dawn Earl; David J. Eckstein; Lisa T. Emrick; Christine M. Eng; Cecilia Esteves; Tyra Estwick; Marni Falk; Liliana Fernandez; Carlos Ferreira; Elizabeth L. Fieg; Paul G. Fisher; Brent L. Fogel; Irman Forghani; Laure Fresard; William A. Gahl; Ian Glass; Rena A. Godfrey; Katie Golden-Grant; Alica M. Goldman; David B. Goldstein; Alana Grajewski; Catherine A. Groden; Andrea L. Gropman; Irma Gutierrez; Sihoun Hahn; Rizwan Hamid; Neil A. Hanchard; Kelly Hassey; Nichole Hayes; Frances High; Anne Hing; Fuki M. Hisama; Ingrid A. Holm; Jason Hom; Martha Horike-Pyne; Alden Huang; Yong Huang; Rosario Isasi; Fariha Jamal; Gail P. Jarvik; Jeffrey Jarvik; Suman Jayadev; Jean M. Johnston; Lefkothea Karaviti; Emily G. Kelley; Jennifer Kennedy; Dana Kiley; Isaac S. Kohane; Jennefer N. Kohler; Deborah Krakow; Donna M. Krasnewich; Elijah Kravets; Susan Korrick; Mary Koziura; Joel B. Krier; Seema R. Lalani; Byron Lam; Christina Lam; Brendan C. Lanpher; Ian R. Lanza; C. Christopher Lau; Kimberly LeBlanc; Brendan H. Lee; Hane Lee; Roy Levitt; Richard A. Lewis; Sharyn A. Lincoln; Pengfei Liu; Xue Zhong Liu; Nicola Longo; Sandra K. Loo; Joseph Loscalzo; Richard L. Maas; Ellen F. Macnamara; Calum A. MacRae; Valerie V. Maduro; Marta M. Majcherska; May Christine V. Malicdan; Laura A. Mamounas; Teri A. Manolio; Rong Mao; Kenneth Maravilla; Thomas C. Markello; Ronit Marom; Gabor Marth; Beth A. Martin; Martin G. Martin; Julian A. Martínez-Agosto; Shruti Marwaha; Jacob McCauley; Allyn McConkie-Rosell; Colleen E. McCormack; Alexa T. McCray; Elisabeth McGee; Heather Mefford; J. Lawrence Merritt; Matthew Might; Ghayda Mirzaa; Eva Morava-Kozicz; Paolo M. Moretti; Marie Morimoto; John J. Mulvihill; David R. Murdock; Mariko Nakano-Okuno; Avi Nath; Stan F. Nelson; John H. Newman; Sarah K. Nicholas; Deborah Nickerson; Donna Novacic; Devin Oglesbee; James P. Orengo; Laura Pace; Stephen Pak; J. Carl Pallais; Christina GS. Palmer; Jeanette C. Papp; Neil H. Parker; John A. Phillips III; Jennifer E. Posey; Lorraine Potocki; Barbara N. Pusey; Aaron Quinlan; Wendy Raskind; Archana N. Raja; Genecee Renteria; Chloe M.

Reuter; Lynette Rives; Amy K. Robertson; Lance H. Rodan; Jill A. Rosenfeld; Natalie Rosenwasser; Robb K. Rowley; Maura Ruzhnikov; Ralph Sacco; Jacinda B. Sampson; Susan L. Samson; Mario Saporta; C. Ron Scott; Judy Schaechter; Timothy Schedl; Kelly Schoch; Daryl A. Scott; Prashant Sharma; Vandana Shashi; Jimann Shin; Rebecca Signer; Catherine H. Sillari; Edwin K. Silverman; Janet S. Sinsheimer; Kathy Sisco; Edward C. Smith; Kevin S. Smith; Emily Solem; Lilianna Solnica-Krezel; Rebecca C. Spillmann; Joan M. Stoler; Nicholas Stong; Jennifer A. Sullivan; Kathleen Sullivan; Angela Sun; Shirley Sutton; David A. Sweetser; Virginia Sybert; Holly K. Tabor; Cecelia P. Tamburro; Queenie K.-G. Tan; Mustafa Tekin; Fred Telischi; Willa Thorson; Cynthia J. Tifft; Camilo Toro; Alyssa A. Tran; Brianna M. Tucker; Tiina K. Urv; Adeline Vanderver; Matt Velinder; Dave Viskochil; Tiphanie P. Vogel; Colleen E. Wahl; Stephanie Wallace; Nicole M. Walley; Chris A. Walsh; Melissa Walker; Jennifer Wambach; Jijun Wan; Lee-kai Wang; Michael F. Wangler; Patricia A. Ward; Daniel Wegner; Mark Wener; Tara Wenger; Katherine Wesseling Perry; Monte Westerfield; Matthew T. Wheeler; Jordan Whitlock; Lynne A. Wolfe; Jeremy D. Woods; Shinya Yamamoto; John Yang; Guoyun Yu; Diane B. Zastrow; Chunli Zhao; Stephan Zuchner.

References

Al-Zoubi AM, Efimova EV, Kaithamana S, Martinez O, El-Idrissi Mel A, Dogan RE, et al. Contrasting effects of IG20 and its splice isoforms, MADD and DENN-SV, on tumor necrosis factor alpha-induced apoptosis and activation of caspase-8 and -3. J Biol Chem 2001; 276: 47202–11.

Alazami AM, Patel N, Shamseldin HE, Anazi S, Al-Dosari MS, Alzahrani F, et al. Accelerating novel candidate gene discovery in neurogenetic disorders via whole-exome sequencing of prescreened multiplex consanguineous families. Cell Rep 2015; 10: 148–61.

Alghamdi KA, Alsaedi AB, Aljasser A, Altawil A, Kamal NM. Extended clinical features associated with novel Glis3 mutation: a case report. BMC Endocr Disord 2017; 17: 14.

Anazi S, Maddirevula S, Salpietro V, Asi YT, Alsahli S, Alhashem A, et al. Expanding the genetic heterogeneity of intellectual disability. Hum Genet 2017; 136: 1419–29.

Bae H, Chen S, Roche JP, Ai M, Wu C, Diantonio A, et al. Rab3-GEF controls active zone development at the drosophila neuromuscular junction. eNeuro 2016; 3: ENEURO.0031-16.2016.

Caballero-Benitez A, Moran J. Caspase activation pathways induced by staurosporine and low potassium: role of caspase-2. J Neurosci Res 2003; 71: 383–96.

Chen X, Li C, Izumi T, Ernst SA, Andrews PC, Williams JA. Rab27b localizes to zymogen granules and regulates pancreatic acinar exocytosis. Biochem Biophys Res Commun 2004; 323: 1157–62.

Chiang L, Ngo J, Schechter JE, Karvar S, Tolmachova T, Seabra MC, et al. Rab27b regulates exocytosis of secretory vesicles in acinar epithelial cells from the lacrimal gland. Am J Physiol Cell Physiol 2011; 301: C507–21.

Chow VT, Lee SS. DENN, a novel human gene differentially expressed in normal and neoplastic cells. DNA Seq 1996; 6: 263–73.

Coppola T, Perret-Menoud V, Gattesco S, Magnin S, Pombo I, Blank U, et al. The death domain of Rab3 guanine nucleotide exchange protein in GDP/GTP exchange activity in living cells. Biochem J 2002; 362: 273.

De Pereda JM, Waas WF, Jan Y, Ruoslahti E, Schimmel P, Pascual J. Crystal structure of a human peptidyl-tRNA hydrolase reveals a new fold and suggests basis for a bifunctional activity. J Biol Chem 2004; 279: 8111.

Del Villar K, Miller CA. Down-regulation of DENN/MADD, a TNF receptor binding protein, correlates with neuronal cell death in Alzheimer's disease brain and hippocampal neurons. Proc Natl Acad Sci U S A 2004; 101: 4210.

Dimitri P, Habeb AM, Gurbuz F, Millward A, Wallis S, Moussa K, et al. Expanding the clinical spectrum associated with GLIS3 mutations. J Clin Endocrinol Metab 2015; 100: E1362.

Dimitri P, Warner JT, Minton JA, Patch AM, Ellard S, Hattersley AT, et al. Novel GLIS3 mutations demonstrate an extended multisystem phenotype. Eur J Endocrinol 2011; 164: 437–43.

Efimova EV, Al-Zoubi AM, Martinez O, Kaithamana S, Lu S, Arima T, et al. IG20, in contrast to DENN-SV, (MADD splice variants) suppresses tumor cell survival, and enhances their susceptibility to apoptosis and cancer drugs. Oncogene 2004; 23: 1076–87.

Figueiredo AC, Wasmeier C, Tarafder AK, Ramalho JS, Baron RA, Seabra MC. Rab3GEP is the non-redundant guanine nucleotide exchange factor for Rab27a in melanocytes. J Biol Chem 2008; 283: 23209–16.

Fukuda M. Rab27 effectors, pleiotropic regulators in secretory pathways. Traffic 2013; 14: 949.

Geppert M, Bolshakov VY, Siegelbaum SA, Takei K, De Camilli P, Hammer RE, et al. The role of Rab3A in neurotransmitter release. Nature 1994; 369: 493.

Gomi H, Mori K, Itohara S, Izumi T. Rab27b is expressed in a wide range of exocytic cells and involved in the delivery of secretory granules near the plasma membrane. MBoC 2007; 18: 4377. 86.

Griffiths GS, Grundl M, Leychenko A, Reiter S, Young-Robbins SS, Sulzmaier FJ, et al. Bit-1 mediates integrin-dependent cell survival through activation of the NFkappaB pathway. J Biol Chem 2011; 286: 14713.

Hu H, Kahrizi K, Musante L, Fattahi Z, Herwig R, Hosseini M, et al. Genetics of intellectual disability in consanguineous families. Mol Psychiatry 2019; 24: 1027–39.

Hu H, Matter ML, Issa-Jahns L, Jijiwa M, Kraemer N, Musante L, et al. Mutations in PTRH2 cause novel infantile-onset multisystem disease with intellectual disability, microcephaly, progressive ataxia, and muscle weakness. Ann Clin Transl Neurol 2014; 1: 1024–35.

Imai A, Ishida M, Fukuda M, Nashida T, Shimomura H. MADD/DENN/Rab3GEP functions as a guanine nucleotide exchange factor for Rab27 during granule exocytosis of rat parotid acinar cells. Arch Biochem Biophys 2013; 536: 31–7.

Imai A, Yoshie S, Nashida T, Shimomura H, Fukuda M. The small GTPase Rab27B regulates amylase release from rat parotid acinar cells. J Cell Sci 2004; 117: 1945–53.

Ioannidis NM, Rothstein JH, Pejaver V, Middha S, McDonnell SK, Baheti S, et al. REVEL: an ensemble method for predicting the pathogenicity of rare missense variants. Am J Hum Genet 2016; 99: 877–85.

Jagadeesh KA, Wenger AM, Berger MJ, Guturu H, Stenson PD, Cooper DN, et al. M-CAP eliminates a majority of variants of uncertain significance in clinical exomes at high sensitivity. Nat Genet 2016; 48: 1581–6.

Jan Y, Matter M, Pai JT, Chen YL, Pilch J, Komatsu M, et al. A mitochondrial protein, Bit1, mediates apoptosis regulated by integrins and Groucho/TLE corepressors. Cell 2004; 116: 751–62.

Jetten AM. GLIS1-3 transcription factors: critical roles in the regulation of multiple physiological processes and diseases. Cell Mol Life Sci 2018; 75: 3473–94.

Kairouz-Wahbe R, Biliran H, Luo X, Khor I, Wankell M, Besch-Williford C, et al. Anoikis effector Bit1 negatively regulates Erk activity. Proc Natl Acad Sci U S A 2008; 105: 1528–32.

Kircher M, Witten DM, Jain P, O'Roak BJ, Cooper GM, Shendure J. A general framework for estimating the relative pathogenicity of human genetic variants. Nat Genet 2014; 46: 310. 5.

Kurada BR, Li LC, Mulherkar N, Subramanian M, Prasad KV, Prabhakar BS. MADD, a splice variant of IG20, is indispensable for MAPK activation and protection against apoptosis upon tumor necrosis factor-alpha treatment. J Biol Chem 2009; 284: 13533–41.

Lang T, Jahn R. Core proteins of the secretory machinery. Handbook of experimental pharmacology. Berlin: Springer; 2008. p. 107–27.

Le C, Prasad AN, Rupar CA, Debicki D, Andrade A, Prasad C. Infantile-onset multisystem neurologic, endocrine, and pancreatic disease: case and review. Can J Neurol Sci 2019; 46: 459–63.

Li LC, Sheng JR, Mulherkar N, Prabhakar BS, Meriggioli MN. Regulation of apoptosis and caspase-8 expression in neuroblastoma cells by isoforms of the IG20 gene. Cancer Res 2008; 68: 7352–61.

Lim KM, Yeo WS, Chow VT. Antisense abrogation of DENN expression induces apoptosis of leukemia cells in vitro, causes tumor regression in vivo and alters the transcription of genes involved in apoptosis and the cell cycle. Int J Cancer 2004; 109: 24–37.

Marat AL, Dokainish H, McPherson PS. DENN domain proteins: regulators of Rab GTPases. J Biol Chem 2011; 286: 13791–800.

Matsuno A, Mizutani A, Okinaga H, Takano K, Yamada S, Yamada SM, et al. Functional molecular morphology of anterior pituitary cells, from hormone production to intracellular transport and secretion. Med Mol Morphol 2011; 44: 63–70.

McKenna A, Hanna M, Banks E, Sivachenko A, Cibulskis K, Kernytsky A, et al. The Genome Analysis Toolkit: a MapReduce framework for analyzing next-generation DNA sequencing data. Genome Res 2010; 20: 1297–303.

Miyoshi J, Takai Y. Dual role of DENN/MADD (Rab3GEP) in neurotransmission and neuroprotection. Trends Mol Med 2004; 10: 476–80.

Mizuno K, Tolmachova T, Ushakov DS, Romao M, Abrink M, Ferenczi MA, et al. Rab27b regulates mast cell granule dynamics and secretion. Traffic 2007; 8: 883–92.

Moog U, Kutsche K, Kortum F, Chilian B, Bierhals T, Apeshiotis N, et al. Phenotypic spectrum associated with CASK loss-of-function mutations. J Med Genet 2011; 48: 741–51.

Mulherkar N, Prasad KV, Prabhakar BS. MADD/DENN splice variant of the IG20 gene is a negative regulator of caspase-8 activation. Knockdown enhances TRAIL-induced apoptosis of cancer cells. J Biol Chem 2007; 282: 11715–21.

Mulherkar N, Ramaswamy M, Mordi DC, Prabhakar BS. MADD/DENN splice variant of the IG20 gene is necessary and sufficient for cancer cell survival. Oncogene 2006; 25: 6252–61.

Murakami-Mori K, Mori S, Bonavida B, Nakamura S. Implication of TNF receptor-I-mediated extracellular signal-regulated kinases 1 and 2 (ERK1/2) activation in growth of AIDS-associated Kaposi's sarcoma cells: a possible role of a novel death domain protein MADD in TNF-alpha-induced ERK1/2 activation in Kaposi's sarcoma cells. J Immunol 1999; 162: 3672.

Niwa S, Tanaka Y, Hirokawa N. KIF1Bbeta- and KIF1A-mediated axonal transport of presynaptic regulator Rab3 occurs in a GTP-dependent manner through DENN/MADD. Nat Cell Biol 2008; 10: 1269–79.

Picker-Minh S, Mignot C, Doummar D, Hashem M, Faqeih E, Josset P, et al. Phenotype variability of infantile-onset multisystem neurologic, endocrine, and pancreatic disease IMNEPD. Orphanet J Rare Dis 2016; 11: 52.

Riviere JB, Ramalingam S, Lavastre V, Shekarabi M, Holbert S, Lafontaine J, et al. KIF1A, an axonal transporter of synaptic vesicles, is mutated in hereditary sensory and autonomic neuropathy type 2. Am J Hum Genet 2011; 89: 219–30.

Schievella AR, Chen JH, Graham JR, Lin LL. MADD, a novel death domain protein that interacts with the type 1 tumor necrosis factor receptor and activates mitogen-activated protein kinase. J Biol Chem 1997; 272: 12069–75.

Senee V, Chelala C, Duchatelet S, Feng D, Blanc H, Cossec JC, et al. Mutations in GLIS3 are responsible for a rare syndrome with neonatal diabetes mellitus and congenital hypothyroidism. Nat Genet 2006; 38: 682. 7.

Sharkia R, Shalev SA, Zalan A, Marom-David M, Watemberg N, Urquhart JE, et al. Homozygous mutation in PTRH2 gene causes progressive sensorineural deafness and peripheral neuropathy. Am J Med Genet A 2017; 173: 1051–5.

Sobreira N, Schiettecatte F, Valle D, Hamosh A. GeneMatcher: a matching tool for connecting investigators with an interest in the same gene. Hum Mutat 2015; 36: 928–30.

Stenmark H. Rab GTPases as coordinators of vesicle traffic. Nat Rev Mol Cell Biol 2009; 10: 513–25.

Tanaka M, Miyoshi J, Ishizaki H, Togawa A, Ohnishi K, Endo K, et al. Role of Rab3 GDP/GTP exchange protein in synaptic vesicle trafficking at the mouse neuromuscular junction. MBoC 2001; 12: 1421–30.

Tolmachova T, Abrink M, Futter CE, Authi KS, Seabra MC. Rab27b regulates number and secretion of platelet dense granules. Proc Natl Acad Sci U S A 2007; 104: 5872–7.

Turner A, Li LC, Pilli T, Qian L, Wiley EL, Setty S, et al. MADD knock-down enhances doxorubicin and TRAIL induced apoptosis in breast cancer cells. PLoS One 2013; 8: e56817.

Wada M, Nakanishi H, Satoh A, Hirano H, Obaishi H, Matsuura Y, et al. Isolation and characterization of a GDP/GTP exchange protein specific for the Rab3 subfamily small G proteins. J Biol Chem 1997; 272: 3875–8.

Wiel L, Baakman C, Gilissen D, Veltman JA, Vriend G, Gilissen C. MetaDome: pathogenicity analysis of genetic variants through aggregation of homologous human protein domains. Hum Mutat 2019; 40: 1030.

Yamaguchi K, Tanaka M, Mizoguchi A, Hirata Y, Ishizaki H, Kaneko K, et al. A GDP/GTP exchange protein for the Rab3 small G protein family up-regulates a postdocking step of synaptic exocytosis in central synapses. Proc Natl Acad Sci U S A 2002; 99: 14536–41.

Yoshimura S, Gerondopoulos A, Linford A, Rigden DJ, Barr FA. Family-wide characterization of the DENN domain Rab GDP-GTP exchange factors. J Cell Biol 2010; 191: 367–81.

Zhang J, Zhang K, Qi L, Hu Q, Shen Z, Liu B, et al. DENN domain-containing protein FAM45A regulates the homeostasis of late/multivesicular endosomes. Biochim Biophys Acta Mol Cell Res 2019; 1866: 916–29.

Zhao C, Takita J, Tanaka Y, Setou M, Nakagawa T, Takeda S, et al. Charcot-Marie-Tooth disease type 2A caused by mutation in a microtubule motor KIF1Bbeta. Cell 2001; 105: 587–97.

Zhao S, Torii S, Yokota-Hashimoto H, Takeuchi T, Izumi T. Involvement of Rab27b in the regulated secretion of pituitary hormones. Endocrinology 2002; 143: 1817–24.